

## ASYMPTOTIC ANALYSIS OF BUFFERED CALCIUM DIFFUSION NEAR A POINT SOURCE\*

GREGORY D. SMITH<sup>†</sup>, LONGXIANG DAI<sup>‡</sup>, ROBERT M. MIURA<sup>§</sup>, AND  
ARTHUR SHERMAN<sup>†</sup>

*This manuscript is dedicated to our dear friend and colleague, the late Joel E. Keizer*

**Abstract.** The “domain” calcium ( $\text{Ca}^{2+}$ ) concentration near an open  $\text{Ca}^{2+}$  channel can be modeled as buffered diffusion from a point source. The concentration profiles can be well approximated by hemispherically symmetric steady-state solutions to a system of reaction-diffusion equations. After nondimensionalizing these equations and scaling space so that both reaction terms and the source amplitude are  $O(1)$ , we identify two dimensionless parameters,  $\varepsilon_c$  and  $\varepsilon_b$ , that correspond to the diffusion coefficients of dimensionless  $\text{Ca}^{2+}$  and buffer, respectively.

Using perturbation methods, we derive approximations for the  $\text{Ca}^{2+}$  and buffer profiles in three asymptotic limits: (1) an “excess buffer approximation” (EBA), where the mobility of buffer exceeds that of  $\text{Ca}^{2+}$  ( $\varepsilon_b \gg \varepsilon_c$ ) and the fast diffusion of buffer toward the  $\text{Ca}^{2+}$  channel prevents buffer saturation (cf. Neher [*Calcium Electrogenesis and Neuronal Functioning*, Exp. Brain Res. 14, Springer-Verlag, Berlin, 1986, pp. 80–96]); (2) a “rapid buffer approximation” (RBA), where the diffusive time-scale for  $\text{Ca}^{2+}$  and buffer are comparable, but slow compared to reaction ( $\varepsilon_c \ll 1$ ,  $\varepsilon_b \ll 1$ , and  $\varepsilon_c/\varepsilon_b = O(1)$ ), resulting in saturation of buffer near the  $\text{Ca}^{2+}$  channel (cf. Wagner and Keizer [*Biophys. J.*, 67 (1994), pp. 447–456] and Smith [*Biophys. J.*, 71 (1996), pp. 3064–3072]); and (3) a new “immobile buffer approximation” (IBA) where the diffusion of buffer is slow compared to that of  $\text{Ca}^{2+}$  ( $\varepsilon_b \ll \varepsilon_c$ ).

To leading order, the EBA and RBA presented here recover results previously obtained by Neher (1986) and Keizer and coworkers (Wagner and Keizer, 1994; Smith, 1996), respectively, while the IBA corresponds to unbuffered diffusion of  $\text{Ca}^{2+}$ . However, the asymptotic formalism allows derivation for the first time of higher order terms, which are shown numerically to significantly extend the range of validity of these approximations. We show that another approximation, derived by linearization rather than by asymptotic approximation (Stern [*Cell Calcium*, 13 (1992), pp. 183–192], Pape, Jong, and Chandler [*J. Gen. Physiol.*, 106 (1995), pp. 259–336], and Naraghi and Neher [*J. Neurosci.*, 17 (1997), pp. 6961–6973]), interpolates between the EBA and IBA solutions. Finally, we indicate where in the  $(\varepsilon_c, \varepsilon_b)$ -plane each of the approximations is accurate and show how the validity of each depends not only on buffer parameters but also on source strength.

**Key words.** calcium domain; calcium buffer; reaction-diffusion equation; rapid, excess, and immobile buffer approximations

**AMS subject classifications.** 92C05, 92C20, 34B15, 34E10, 35K57

**PII.** S0036139900368996

---

\*Received by the editors March 10, 2000; accepted for publication (in revised form) August 16, 2000; published electronically March 20, 2001. This work was performed by an employee of the U.S. Government or under U.S. Government contract. The U.S. Government retains a nonexclusive, royalty-free license to publish or reproduce the published form of this contribution, or allow others to do so, for U.S. Government purposes. Copyright is owned by SIAM to the extent not limited by these rights.

<http://www.siam.org/journals/siap/61-5/36899.html>

<sup>†</sup>Department of Mathematics, Arizona State University, Tempe, AZ 85287-1804 (greg@math.la.asu.edu). The work of this author was supported in part by an NIH Intramural Research Training Assistantship and NEI National Research Service Award EY06903-01.

<sup>‡</sup>Mathematical Research Branch, National Institute of Diabetes and Digestive and Kidney Diseases, National Institute of Health, 9190 Wisconsin Ave., Suite 350, Bethesda, MD 20814 (lxdai@yahoo.com, sherman@helix.nih.gov).

<sup>§</sup>Department of Mathematics, Institute of Applied Mathematics, and Department of Pharmacology and Therapeutics, University of British Columbia, Vancouver, B.C., Canada V6T 1Z2 (miura@math.ubc.ca). The work of this author was supported in part by a grant from the Natural Sciences and Engineering Research Council of Canada.

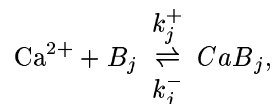
**1. Introduction.** A deep understanding of the dynamics of calcium ( $\text{Ca}^{2+}$ ) is very important in cellular physiology because  $\text{Ca}^{2+}$  binds to many proteins and regulates their activity and interactions [1, 2, 6]. Calcium mediates many hormonal responses and is important in secretion of hormones and neurotransmitters, in muscle contraction, and in the regulation of gene expression. Because  $\text{Ca}^{2+}$  is a ubiquitous signaling agent and is toxic in high concentrations, it is highly buffered by  $\text{Ca}^{2+}$ -binding proteins, so that less than 1% of the  $\text{Ca}^{2+}$  in cells exists in a free ionic form. This helps to confine large excursions in concentration to well-localized regions and contributes to specificity of signaling. The targets that bind  $\text{Ca}^{2+}$  include secretory vesicles,  $\text{Ca}^{2+}$ -activated  $K^+$  channels, and the channels that themselves conduct  $\text{Ca}^{2+}$  through membranes. These targets are located very near the sources of  $\text{Ca}^{2+}$ , often within tens of nanometers. This is close enough that steady states are achieved within microseconds [10, 11, 15]. In contrast,  $\text{Ca}^{2+}$ -regulated cellular processes typically operate on a time-scale of milliseconds. Thus, though not a complete description for all cases, it is of interest to examine steady-state solutions. For simplicity, we consider only isolated  $\text{Ca}^{2+}$  sources and one species of buffer.

Approximate solutions have been derived for this case in the biophysical literature and are described in section 3. We show in sections 5 and 6 that two of these approximate solutions correspond to leading-order solutions of the equations in different asymptotic regimes. These regimes are defined in terms of two dimensionless parameters identified in section 4, where we nondimensionalize the equations and scale space so that the reaction terms and the source amplitude are  $O(1)$ . The dimensionless parameters ( $\varepsilon_c$  and  $\varepsilon_b$ ) correspond to the scaled diffusion coefficients of dimensionless  $\text{Ca}^{2+}$  and buffer, respectively.

In addition to putting the results in the literature on a more rigorous basis, with this approach, we are able to extend the excess and rapid buffer approximations to higher order. In section 7, we derive to first and second order another approximation, which we interpret as a (nearly) immobile buffer approximation. Refer to Table 3.1 for a synopsis of the various approximations discussed in this manuscript and when they first appeared in the literature.

Another approximation based on linearizing the equations is discussed in section 8. In section 9, we compare the asymptotic approximations (EBA, RBA, IBA) and the linearized approximation (LIN) to numerically calculated steady-state solutions of the full equations. The quantitative error analysis confirms the asymptotic analysis and clarifies the regions of validity of the four approximations in terms of the two dimensionless parameters of the problem,  $\varepsilon_c$  and  $\varepsilon_b$ .

**2. Formulation of the reaction-diffusion problem.** The buffered diffusion of  $\text{Ca}^{2+}$  near isolated point sources can be described mathematically by a system of reaction-diffusion equations with spherical symmetry. (In some respects, a stochastic description may be more appropriate because of the small number of  $\text{Ca}^{2+}$  ions, but we use deterministic equations in order to obtain analytical results.) It is standard to assume homogeneity, isotropy, and Fickian diffusion as well as bimolecular association reactions between  $\text{Ca}^{2+}$  and buffer of the form



where  $B_j$  and  $CaB_j$  are free and bound buffer, respectively, and  $j$  is an index over the buffer species. With these assumptions, it is straightforward to write the following

system of reaction-diffusion equations for the concentrations of free  $\text{Ca}^{2+}$ , free buffer ( $[B_j]$ ), and bound buffer ( $[CaB_j]$ ), respectively [21]:

$$(2.1) \quad \frac{\partial[Ca^{2+}]}{\partial t} = D_{Ca} \nabla^2[Ca^{2+}] + \sum_j R_j,$$

$$(2.2) \quad \frac{\partial[B_j]}{\partial t} = D_{B_j} \nabla^2[B_j] + R_j,$$

$$(2.3) \quad \frac{\partial[CaB_j]}{\partial t} = D_{CaB_j} \nabla^2[CaB_j] - R_j,$$

with the reaction terms given by

$$(2.4) \quad R_j = -k_j^+[B_j][Ca^{2+}] + k_j^- [CaB_j].$$

In these equations,  $D_{Ca}$ ,  $D_{B_j}$ , and  $D_{CaB_j}$  are diffusion coefficients for free  $\text{Ca}^{2+}$ , free buffer, and bound buffer, respectively;  $k_j^+$  and  $k_j^-$  are the association and dissociation rate constants for buffer  $j$ , respectively. Buffers that do not diffuse are referred to as stationary, immobile, or fixed and are accounted for by setting  $D_{B_j} = D_{CaB_j} = 0$ .

For boundary conditions, we assume a point source of  $\text{Ca}^{2+}$  at the origin and a fixed background  $\text{Ca}^{2+}$  concentration. There are no sources for buffer, and the buffer is assumed to be in equilibrium with  $\text{Ca}^{2+}$  far from the source. The corresponding equations are

$$\begin{aligned} \lim_{r \rightarrow 0} \left\{ -2\pi r^2 D_{Ca} \frac{d[Ca^{2+}]}{dr} \right\} &= \sigma, & \lim_{r \rightarrow \infty} [Ca^{2+}] &= [Ca^{2+}]_\infty, \\ \lim_{r \rightarrow 0} \left\{ -2\pi r^2 D_{B_j} \frac{d[B_j]}{dr} \right\} &= 0, & \lim_{r \rightarrow \infty} [B_j] &= [B_j]_\infty, \\ \lim_{r \rightarrow 0} \left\{ -2\pi r^2 D_{CaB_j} \frac{d[CaB_j]}{dr} \right\} &= 0, & \lim_{r \rightarrow \infty} [CaB_j] &= [CaB_j]_\infty, \end{aligned}$$

where

$$[B_j]_\infty = \frac{K_j [B_j]_T}{K_j + [Ca^{2+}]_\infty}, \quad [CaB_j]_\infty = \frac{[Ca^{2+}]_\infty [B_j]_T}{K_j + [Ca^{2+}]_\infty},$$

$K_j = k_j^-/k_j^+$  is the dissociation constant for buffer  $j$ , and  $[B_j]_T = [B_j] + [CaB_j]$  is the total concentration profile of each buffer. The factor  $2\pi$  reflects the fact that  $[Ca^{2+}]$  is diffusing into a hemisphere. In the literature one often finds  $4\pi$ , which is equivalent provided  $\sigma$  is set equal to twice the physical source strength. In this paper  $\sigma$  always represents the physical source strength.

If we further assume that the diffusion constant of each mobile buffer is not affected by the binding of  $\text{Ca}^{2+}$  (that is,  $D_{B_j} = D_{CaB_j}$ ), and also assume that  $[B_j]_T$  is initially uniform, then  $[B_j]_T$  will remain uniform for all time. Thus we can omit (2.3) and rewrite (2.4) as

$$R_j = -k_j^+[B_j][Ca^{2+}] + k_j^- ([B_j]_T - [B_j]).$$

As motivated in section 1, we restrict consideration to steady-state solutions, that is, to the “domains” of high  $\text{Ca}^{2+}$ , which are established within microseconds near sources.

Note that for fixed buffers,  $D_{B_j} = D_{CaB_j} = 0$  in (2.1)–(2.3), so the  $R_j = 0$  in the steady state. Thus, if all the buffers are fixed, then the steady-state  $[Ca^{2+}]$  distribution is the unbuffered steady-state solution. For mobile buffers, on the other hand, the reaction terms are not zero in general at steady state; net production of buffer at a point in space can be balanced by diffusion of free buffer away from that point if there is a standing gradient. Although we will not consider time-dependent solutions here, fixed buffers do have a big influence in that case—for example, slowing the approach to the steady state.

Finally, for simplicity, we assume a single mobile buffer species,  $[B]$ , resulting in the following boundary-value problem:

$$(2.5) \quad 0 = D_c \nabla^2 [Ca^{2+}] - k^+ [B][Ca^{2+}] + k^- ([B]_T - [B]),$$

$$(2.6) \quad 0 = D_b \nabla^2 [B] - k^+ [B][Ca^{2+}] + k^- ([B]_T - [B]),$$

with the boundary conditions

$$(2.7) \quad \begin{aligned} \lim_{r \rightarrow 0} \left\{ -2\pi r^2 D_c \frac{d[Ca^{2+}]}{dr} \right\} &= \sigma, & \lim_{r \rightarrow \infty} [Ca^{2+}] &= [Ca^{2+}]_\infty, \\ \lim_{r \rightarrow 0} \left\{ -2\pi r^2 D_b \frac{d[B]}{dr} \right\} &= 0, & \lim_{r \rightarrow \infty} [B] &= [B]_\infty = \frac{K[B]_T}{K + [Ca^{2+}]_\infty}. \end{aligned}$$

For notational simplicity, we have written  $D_c$  and  $D_b$  for the diffusion coefficients of free  $Ca^{2+}$  and free buffer, respectively, and  $\nabla^2$  as an abbreviation for

$$\nabla^2 = \frac{1}{r^2} \frac{d}{dr} \left[ r^2 \frac{d}{dr} \right].$$

The remainder of the paper is devoted to approximate solutions of the steady-state equations for buffered  $Ca^{2+}$  diffusion (2.5)–(2.7).

**3. Survey of prior results.** Beginning with the model problem (2.5)–(2.7), several investigators have derived approximate solutions in different limiting parameter regimes. Since the results presented here are an extension of these ideas, we will briefly review this previous work; see Table 3.1.

**3.1. The excess buffer approximation (EBA).** In his seminal work, Neher [12] made the critical observation that if buffer is present in excess, then the free mobile buffer profile is not perturbed by the presence of the source. Under this assumption, one can make the approximation that  $[B] \approx [B]_\infty$  in (2.5), yielding

$$(3.1) \quad 0 = D_c \nabla^2 [Ca^{2+}] - k^+ [B]_\infty [Ca^{2+}] + k^- ([B]_T - [B]_\infty).$$

Then (2.6) is approximated by

$$k^- ([B]_T - [B]_\infty) = k^+ [B]_\infty [Ca^{2+}]_\infty,$$

so (3.1) becomes

$$0 = D_c \nabla^2 [Ca^{2+}] - k^+ [B]_\infty ([Ca^{2+}] - [Ca^{2+}]_\infty).$$

This linear equation for  $[Ca^{2+}]$  can be solved easily and applying the boundary conditions (2.7) gives [4, 7]

$$(3.2) \quad [Ca^{2+}] = \frac{\sigma}{2\pi D_c r} e^{-r/\lambda} + [Ca^{2+}]_\infty,$$

TABLE 3.1

Relevant references to the different approximate steady-state solutions to the equations for the buffered diffusion of  $\text{Ca}^{2+}$ . Entries labeled THIS MANUSCRIPT are presented here for the first time.

Approximation	1st order	2nd order
excess buffer approximation	Neher 1986 [12]	THIS MANUSCRIPT
	Stern 1992 [20]	
rapid buffer approximation	Wagner and Keizer 1994 [21]	THIS MANUSCRIPT
	Smith 1996 [16]	
immobile buffer approximation	THIS MANUSCRIPT	THIS MANUSCRIPT
	Stern 1992 [20]	
linearization	Pape et al. 1995 [14]	N/A
	Naraghi and Neher 1997 [11]	

where  $\lambda$  is the characteristic length constant for the mobile  $\text{Ca}^{2+}$  buffer given by  $\lambda = \sqrt{D_c/k^+[B]_\infty}$ . This approximation has been shown to be valid when mobile buffer is in high concentration and/or when the source amplitude is small, that is,  $\lim_{r \rightarrow 0} [B] \approx [B]_\infty$  [12, 17].

**3.2. The rapid buffer approximation (RBA).** Whereas the heuristic behind the EBA is linearizing the equations by assuming the free buffer is constant, the RBA is based on setting the reaction terms, thought to be fast, to equilibrium. In the course of studying the effects of buffers on  $\text{Ca}^{2+}$  waves, Wagner and Keizer [21] derived the following single nonlinear transport equation in lieu of the system (2.1)–(2.4):

$$(3.3) \quad \frac{\partial [Ca^{2+}]}{\partial t} = \alpha \left[ (D_c + \kappa D_b) \nabla^2 [Ca^{2+}] - \frac{2\kappa D_b}{K + [Ca^{2+}]} \nabla [Ca^{2+}] \cdot \nabla [Ca^{2+}] \right],$$

where  $\alpha = (1 + \kappa)^{-1}$ ,  $\kappa = K[B]_T / (K + [Ca^{2+}])^2$ , and  $K = k^-/k^+$ . The same equation, but without the transport term, appeared in [22] and was applied to one-dimensional neuronal processes. Sneyd, Dale, and Duffy [19] derived a change of variables that transforms (3.3) to a one-variable reaction-diffusion equation with nonlinear diffusion coefficient and no transport term.

For a single buffer, an explicit steady-state solution was obtained in [16] by directly integrating (3.3):

$$(3.4) \quad [Ca^{2+}] = \frac{1}{2D_c} \left( -D_c K + \frac{\sigma}{2\pi r} + D_c [Ca^{2+}]_\infty - D_b [B]_\infty \right. \\ \left. + \sqrt{\left( D_c K + \frac{\sigma}{2\pi r} + D_c [Ca^{2+}]_\infty - D_b [B]_\infty \right)^2 + 4D_c D_b [B]_T K} \right).$$

Stern [20] had observed previously that the steady-state equations (2.5) and (2.6) could be simplified and solved analytically when the reaction rates are large. The steady-state formula (3.4) was extended to multiple sources in [3].

Wagner and Keizer [21] argued that the RBA would be valid provided that reaction is fast compared to the diffusive time-scale,  $T_{diff} = L_{wave}^2/D_c$ , where  $L_{wave}$  is the thickness of the wave-front. For a point source with spherical symmetry, the conditions of validity are different and are described fully below. It already has been recognized from numerical studies that a strong source (as well as fast binding rates) is important for the validity of the RBA [17]. The fundamental assumption used

in deriving both (3.3) and (3.4) is that buffer and  $\text{Ca}^{2+}$  are in pointwise equilibrium in space, a condition called *local equilibrium*. This, combined with the fact that  $[Ca^{2+}] \rightarrow \infty$  as  $r \rightarrow 0$  in (3.4), implies  $\lim_{r \rightarrow 0} [B] = 0$ . Thus, the steady-state RBA cannot be valid unless the source is strong enough to saturate the buffer. Since in the EBA the buffer is assumed not to be perturbed even at the source, the EBA and RBA approximations are complementary.

**3.3. Linearization.** A number of authors [11, 14, 20] have derived approximate steady-state solutions to (2.5)–(2.7) by linearizing the reaction-diffusion system around the equilibrium values,  $[B]_\infty$  and  $[Ca^{2+}]_\infty$  (for a review see [13]). Thus, defining  $\delta[Ca^{2+}] = [Ca^{2+}] - [Ca^{2+}]_\infty$  and  $\delta[B] = [B] - [B]_\infty$ , substituting in (2.5)–(2.7), and keeping only linear terms leads to a system of linear ODEs that can be solved to give

$$(3.5) \quad [Ca^{2+}] = [Ca^{2+}]_\infty + \frac{\sigma}{2\pi r (D_c + \kappa_\infty D_b)} \left[ 1 + \frac{\kappa_\infty D_b}{D_c} e^{-r/\lambda} \right],$$

$$(3.6) \quad [B] = [B]_\infty + \frac{\sigma \kappa_\infty}{2\pi r (D_c + \kappa_\infty D_b)} \left[ e^{-r/\lambda} - 1 \right],$$

where

$$\frac{1}{\lambda^2} = \frac{1}{\tau} \left( \frac{1}{D_b} + \frac{\kappa_\infty}{D_c} \right),$$

$$\frac{1}{\tau} = k^+ [Ca^{2+}]_\infty + k^-,$$

and

$$(3.7) \quad \kappa_\infty = \frac{K[B]_T}{(K + [Ca^{2+}]_\infty)^2}.$$

Naraghi and Neher [11] extended and applied this method to the case of multiple buffers. The  $\kappa_\infty$  here is the same as the  $\kappa$  in (3.3), evaluated at  $[Ca^{2+}]_\infty$ . When  $\kappa_\infty$  is large, its reciprocal is approximately the fraction of  $[Ca^{2+}]$  which is unbound, typically less than 0.01. For large  $\kappa_\infty$ , (3.5) reduces to the EBA solution for  $[Ca^{2+}]$ , (3.2). In the same limit, (3.6) gives an improvement to the original EBA approximation for buffer that allows for partial saturation.

As can be seen,  $\delta[Ca^{2+}]$  does not remain small but becomes unbounded as  $r \rightarrow 0$ , so this linearization procedure requires justification. In section 8, we discuss under what conditions it is valid.

**4. Nondimensionalization.** We begin the original work in this paper by nondimensionalizing the dependent variables of (2.5)–(2.7),  $[Ca^{2+}]$  and  $[B]$ , by scaling by representative concentrations, the dissociation constant of the buffer ( $K$ ) and the total concentration of buffer ( $[B]_T$ ), respectively. Thus, the dimensionless free  $\text{Ca}^{2+}$  is given by  $c = [Ca^{2+}]/K$  ( $c_\infty = [Ca^{2+}]_\infty/K$ ) and dimensionless free buffer by  $b = [B]/[B]_T$  ( $b_\infty = [B]_\infty/[B]_T$ ). Define the scaled independent variable  $\rho = r/L$ , so the boundary condition (2.7) for  $c$  near the source becomes

$$\lim_{\rho \rightarrow 0} \left\{ -\rho^2 \frac{dc}{d\rho} \right\} = \frac{\sigma}{2\pi D_c K L},$$

where  $L$  is chosen so that the right-hand side of this expression is unity, i.e.,

$$(4.1) \quad L = \frac{\sigma}{2\pi D_c K}.$$

Using this nondimensionalization, (2.5) and (2.6) simplify to

$$(4.2) \quad \varepsilon_c \nabla_\rho^2 c - (cb + b - 1) = 0,$$

$$(4.3) \quad \varepsilon_b \nabla_\rho^2 b - (cb + b - 1) = 0,$$

where the subscript on the Laplacian indicates that the differentiation is with respect to  $\rho$ . The dimensionless diffusion coefficients for the dimensionless free  $\text{Ca}^{2+}$  and buffer are given by

$$(4.4) \quad \varepsilon_c = \frac{(2\pi)^2 D_c^3 K^2}{\sigma^2 k^+ [B]_T},$$

$$(4.5) \quad \varepsilon_b = \frac{(2\pi)^2 D_c^2 D_b K}{\sigma^2 k^+}.$$

Thus, the boundary conditions (2.7) become

$$(4.6) \quad \lim_{\rho \rightarrow 0} \left\{ -\rho^2 \frac{dc}{d\rho} \right\} = 1, \quad \lim_{\rho \rightarrow \infty} c = c_\infty,$$

$$(4.7) \quad \lim_{\rho \rightarrow 0} \left\{ -\rho^2 \frac{db}{d\rho} \right\} = 0, \quad \lim_{\rho \rightarrow \infty} b = b_\infty = \frac{1}{1 + c_\infty}.$$

The reader may find it of interest to compare the nondimensionalization with the informal scaling analysis of Roberts [15].

It will be convenient for calculation and interpretation to define alternative dimensionless constants by regrouping the factors that  $\varepsilon_c$  and  $\varepsilon_b$  have in common. Define

$$(4.8) \quad \varepsilon = \frac{(2\pi)^2 D_c^3 K}{\sigma^2 k^+},$$

the buffering factor  $\beta$ ,

$$(4.9) \quad \beta = \frac{K}{[B]_T},$$

and the ratio of the diffusion coefficients  $D$ ,

$$(4.10) \quad D = \frac{D_b}{D_c}.$$

Then  $\varepsilon_c = \varepsilon\beta$  and  $\varepsilon_b = \varepsilon D$ .

**4.1. Physiological values for dimensionless parameters and representative profiles.** Nondimensionalization has reduced the seven parameters of the original problem ( $k^+$ ,  $k^-$ ,  $[B]_T$ ,  $[Ca^{2+}]_\infty$ ,  $D_c$ ,  $D_b$ ,  $\sigma$ ) to three ( $\varepsilon_c$ ,  $\varepsilon_b$ ,  $c_\infty$ ). The first two parameters are the diffusion coefficients described above. The third parameter  $c_\infty$  appears in the boundary conditions for  $\text{Ca}^{2+}$  and buffer far from the source. It appears in the solution as an additive constant, and through its influence on  $b_\infty$  (4.7). Typically,  $c_\infty \ll 1$  and is not important. Therefore, we focus on parameters  $\varepsilon_c$  and  $\varepsilon_b$ .

TABLE 4.1  
Table of parameters for  $\text{Ca}^{2+}$ -binding species used in Figure 4.1.

Buffer	$D_b$ ( $\mu\text{m}^2/\text{s}$ )	$k^+$ ( $\mu\text{M}^{-1}\text{s}^{-1}$ )	$k^-$ ( $\text{s}^{-1}$ )	$K$ ( $\mu\text{M}$ )
BAPTA	95	600	100	0.17
EGTA	113	1.5	0.3	0.2
ENDO G	15	500	5000	10

TABLE 4.2  
Physiological values of  $\varepsilon_c$  and  $\varepsilon_b$  used in Figure 4.1. The dimensionless parameters  $\varepsilon_c$  and  $\varepsilon_b$  are calculated according to (4.4) and (4.5) using the values of total mobile buffer concentration,  $[B]_T$ , and current amplitude,  $i_{\text{Ca}}$ , shown below in combination with buffer parameters shown in Table 4.1. Also shown are dimensionless parameters,  $\varepsilon$ ,  $\beta$ , and  $D$ , calculated using (4.8), (4.9), and (4.10), respectively. Calculation of  $D$  assumes  $D_c = 250 \mu\text{m}^2/\text{s}$ . Membrane current,  $i_{\text{Ca}}$ , of 1.0 pA corresponds to source amplitude,  $\sigma$ , of  $5.1824 \times 10^{-12} \mu\text{moles}/\text{s}$ , using Faraday's law,  $\sigma = i_{\text{Ca}}/zF$ , where  $z = 2$  is the valence of  $\text{Ca}^{2+}$  and  $F = 9.648 \times 10^4 \text{ coul}/\text{mol}$ .

	Symbol in Figure 4.1	$[B]_T$ ( $\mu\text{M}$ )	$i_{\text{Ca}}$ (pA)	$\varepsilon$	$\beta$	$D$	$\varepsilon_c$	$\varepsilon_b$
BAPTA	*	100	0.05	2.55	0.00167	0.38	0.00425	0.97
	o	1000	0.05	2.55	0.000167	0.38	0.000425	0.97
	◇	100	0.5	0.0255	0.00167	0.38	4.25e-05	0.0097
EGTA	*	100	0.05	1220	0.002	0.452	2.45	554
	o	1000	0.05	1220	0.0002	0.452	0.245	554
	◇	100	0.5	12.2	0.002	0.452	0.0245	5.54
ENDO G	*	100	0.05	184	0.1	0.06	18.4	11
	o	1000	0.05	184	0.01	0.06	1.84	11
	◇	100	0.5	1.84	0.01	0.06	0.184	0.11

Table 4.1 shows experimental estimates of the dimensional parameters for three representative  $\text{Ca}^{2+}$ -binding species: two exogenous  $\text{Ca}^{2+}$  chelators used in experiments, namely, BAPTA, a fast, high-affinity mobile buffer, and EGTA, a slow high-affinity mobile buffer. In addition, ENDO G refers to an endogenous buffer with low mobility using properties estimated for a neuroendocrine cell [10]. In Table 4.2,  $\varepsilon_c$  and  $\varepsilon_b$  are estimated for several values of the source amplitude and total buffer concentration and plotted in the  $(\varepsilon_c, \varepsilon_b)$ -plane of Figure 4.1. In agreement with (4.4) and (4.5), increasing buffer concentration decreases  $\varepsilon_c$  but has no effect on  $\varepsilon_b$  (horizontal lines in Figure 4.1). This conforms to the intuition that increased buffer reduces the mobility of  $\text{Ca}^{2+}$ . On the other hand, increasing the  $\text{Ca}^{2+}$  source amplitude causes a reduction in both  $\varepsilon_c$  and  $\varepsilon_b$  (diagonal lines in Figure 4.1). This reflects the fact that in our scaling, increasing  $\sigma$ , like increasing reaction rate  $k^+$ , has the effect of slowing the diffusion of both species compared to reaction.

The graphs labeled 0.05 pA and 0.5 pA in Figure 4.1 show  $\text{Ca}^{2+}$  and buffer profiles for two particular choices of  $\varepsilon_c$  and  $\varepsilon_b$  (see ENDO G \* and ◇ in Table 4.2). In both cases, the buffer parameters used represent 100  $\mu\text{M}$  of “endogenous” buffer [10] (see Table 4.1). Note that in the case of a 0.05 pA source, the buffer profile is relatively unperturbed, consistent with the EBA, while in the case of a 0.5 pA source, the buffer profile approaches a small value for small  $\rho$ , consistent with the RBA. In the case of the strong versus weak source, the  $\text{Ca}^{2+}$  domains in Figure 4.1 are of similar size in units of dimensionless space,  $\rho$ . However,  $L$  (cf. (4.1)) is 0.0165  $\mu\text{m}$  in the weak source case and 0.165  $\mu\text{m}$  in the strong source case, and when these different scalings of dimensional space,  $r$ , are accounted for, the 0.5 pA  $\text{Ca}^{2+}$  domain is approximately 10 times larger than the 0.05 pA domain. Both cases were calculated with  $[Ca^{2+}]_\infty$

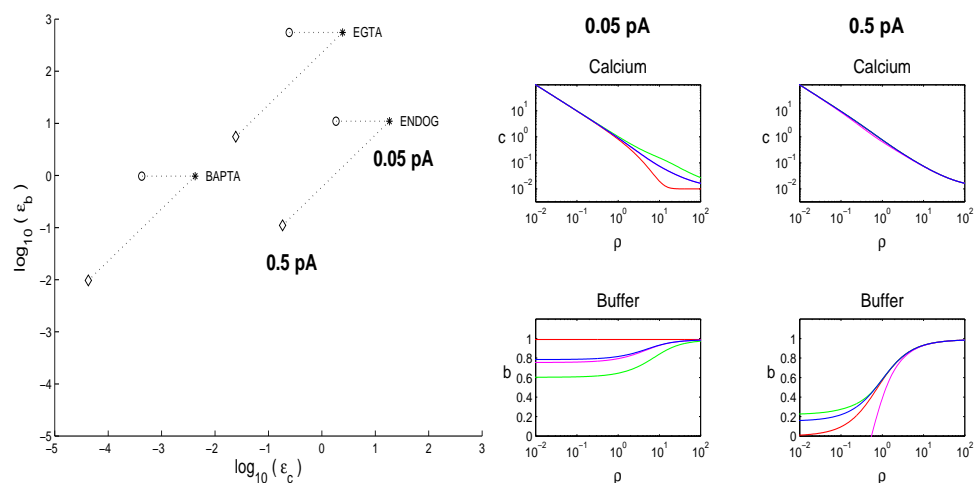


FIG. 4.1. Estimated values of dimensionless parameters  $\varepsilon_c$  and  $\varepsilon_b$  for several different  $\text{Ca}^{2+}$ -binding species, including the exogenous  $\text{Ca}^{2+}$  chelators, EGTA and BAPTA, and a low-affinity buffer, ENDOG, with properties based on estimates for endogenous buffer in adrenal chromaffin cells [10]. The values of  $\varepsilon_c$  and  $\varepsilon_b$  depend strongly on total buffer concentration and source amplitude, so the positions in the  $(\varepsilon_c, \varepsilon_b)$ -plane for each  $\text{Ca}^{2+}$ -binding species are plotted for three different combinations of  $[B]_T$  (in  $\mu\text{M}$ ) and current amplitude,  $i_{\text{Ca}}$  (in pA): \*, 100 and 0.05;  $\circ$ , 1000 and 0.05;  $\diamond$ , 100 and 0.5. See Tables 4.1, 4.2 for numerical values. Profiles of dimensionless  $\text{Ca}^{2+}$  ( $c$ ) and free buffer ( $b$ ) are shown for a 0.05 and 0.5 pA source. The blue lines represent the numerically calculated solution of the full equations, (4.2) and (4.3); red and green lines are first- and second-order EBA for the weak source and first- and second-order RBA for the strong source; magenta lines are the solutions of the linearized equations, (8.3) and (8.4).

fixed at 0.1  $\mu\text{M}$ , so that  $c_\infty$  is 0.01.

**5. The EBA.** Physically, the essence of the EBA is that the buffer is not saturated, even at the source. In section 3.1, we pointed out that this assumption leads to a linear equation with a simple solution (3.2). High buffer concentration minimizes saturation, but the mobility of the buffer is also important. Stationary buffers, even at high concentrations, will eventually be saturated near a source. The key is whether sufficient mobile buffer can diffuse to the source to replenish the free buffer that becomes bound. This motivates consideration of a regime in which the mobility of  $b$  is much greater than that of  $c$  in (4.2) and (4.3).

Therefore, we consider in detail the case  $\varepsilon_c = O(1)$ ,  $\varepsilon_b \gg 1$ . In this regime, the diffusion coefficient of  $c$  is comparable to the reaction terms, while the diffusion coefficient of  $b$  is much larger than the reaction terms. Because  $\varepsilon_b = \varepsilon_c D / \beta$ , one way that this could occur is if  $D = O(1)$  while  $\beta \ll 1$ , that is,  $[B]_T \gg K$ . This is the connection to the original notion of excess buffer. Note, however, that  $\varepsilon_c = O(1)$  implies also that the source strength ( $\sigma$ ) is not too large (4.4). Similar results obtain when  $\varepsilon_b = O(1)$ ,  $\varepsilon_c \ll 1$ .

Let  $\mu \equiv \beta / D = \varepsilon_c / \varepsilon_b$  be the small parameter. Then, (4.2) and (4.3) become the regularly perturbed system

$$(5.1) \quad \varepsilon_c \nabla_\rho^2 c - (cb + b - 1) = 0,$$

$$(5.2) \quad \varepsilon_c \nabla_\rho^2 b - \mu (cb + b - 1) = 0.$$

We assume  $c$  and  $b$  have perturbation expansions for small  $\mu$  of the form

$$\begin{aligned}c &= c_0 + \mu c_1 + \mu^2 c_2 + \cdots, \\b &= b_0 + \mu b_1 + \mu^2 b_2 + \cdots\end{aligned}$$

and obtain the leading-order equations

$$(5.3) \quad \varepsilon_c \nabla^2 c_0 - (c_0 b_0 + b_0 - 1) = 0,$$

$$(5.4) \quad \nabla^2 b_0 = 0.$$

Equation (5.4), together with the leading-order boundary conditions for  $c_0$  (4.6) and  $b_0$  (4.7) as  $\rho \rightarrow \infty$ , gives

$$(5.5) \quad b_0 = b_\infty,$$

where  $b_\infty = 1/(1 + c_\infty)$  (4.7). Thus, the assumption in prior work that the buffer is not perturbed from its rest value when it is present in excess is derived here as the leading-order approximation for  $b$ . Substituting (5.5) into (5.3) gives

$$\varepsilon_c \nabla^2 c_0 - b_\infty (c_0 - c_\infty) = 0,$$

with the boundary conditions

$$(5.6) \quad \lim_{\rho \rightarrow 0} \left\{ -\rho^2 \frac{dc_0}{d\rho} \right\} = 1, \quad \lim_{\rho \rightarrow \infty} c_0 = c_\infty,$$

and solution

$$(5.7) \quad c_0 = c_\infty + \frac{1}{\rho} e^{-\rho/\Lambda},$$

where the dimensionless space constant  $\Lambda = \sqrt{\varepsilon_c/b_\infty}$ . This is Neher's result (3.2) expressed in dimensionless form.

**5.1. Second-order results.** The second-order equation for  $c_1$  is

$$(5.8) \quad \varepsilon_c \nabla^2 c_1 - (c_1 b_0 + c_0 b_1 + b_1) = 0.$$

Combining (5.1) and (5.2) gives a relationship,

$$(5.9) \quad \nabla_\rho^2 [\mu c - b] = 0,$$

which will enable us to eliminate  $b_1$  in (5.8). Expanding (5.9) in powers of  $\mu$ , we obtain a recursion relation

$$c_i - b_{i+1} = \frac{A_1^i}{\rho} + A_0^i$$

that gives  $b_{i+1}$  in terms of  $c_i$ . The  $A_1^i$  and  $A_0^i$  are constants to be determined by the boundary conditions at each order. For  $i = 0$ , the boundary conditions for  $c_0$  (5.6) and  $b_1$ ,

$$\lim_{\rho \rightarrow 0} \left\{ -\rho^2 \frac{db_1}{d\rho} \right\} = 0, \quad \lim_{\rho \rightarrow \infty} b_1 = 0,$$

allow us to identify  $A_1^0 = 1$  and  $A_0^0 = c_\infty$ . Thus,

$$b_1 = \frac{1}{\rho} \left( e^{-\rho/\Lambda} - 1 \right),$$

and the second-order equation (5.8) can be written as

$$(5.10) \quad \varepsilon_c \nabla^2 c_1 - \left[ c_1 b_\infty + \left( 1 + c_\infty + \frac{1}{\rho} e^{-\rho/\Lambda} \right) \frac{1}{\rho} \left( e^{-\rho/\Lambda} - 1 \right) \right] = 0.$$

To solve (5.10) for  $c_1$ , we change variables so that  $x = \rho/\Lambda$  and  $C = \rho c_1 = \Lambda x c_1$ :

$$(5.11) \quad C_{xx} = C + \frac{1}{b_\infty} \left( 1 + c_\infty + \frac{1}{\Lambda x} e^{-x} \right) (e^{-x} - 1).$$

Using variation of parameters, the general solution of (5.11) is

$$(5.12) \quad C = \xi(x) e^x + \eta(x) e^{-x},$$

where

$$(5.13) \quad \xi(x) = \frac{1 + c_\infty}{2b_\infty} \left( e^{-x} - \frac{1}{2} e^{-2x} \right) + \frac{1}{2\Lambda b_\infty} \int_0^x \frac{e^{-3y} - e^{-2y}}{y} dy + \xi_0,$$

$$(5.14) \quad \eta(x) = \frac{1 + c_\infty}{2b_\infty} (e^x - x) - \frac{1}{2\Lambda b_\infty} \int_0^x \frac{e^{-y} - 1}{y} dy + \eta_0,$$

and  $\xi_0$  and  $\eta_0$  are constants to be determined by the boundary conditions. This is more easily done by reexpressing (5.12)–(5.14) in terms of  $c_1$ :

$$(5.15) \quad c_1 = \frac{1}{\Lambda x} \left\{ \frac{1 + c_\infty}{2b_\infty} \left[ 2 - \left( \frac{1}{2} + x \right) e^{-x} \right] + \frac{1}{2\Lambda b_\infty} \left[ e^x \int_0^x \frac{e^{-3y} - e^{-2y}}{y} dy - e^{-x} \int_0^x \frac{e^{-y} - 1}{y} dy \right] + \xi_0 e^x + \eta_0 e^{-x} \right\}.$$

The boundary condition (4.6), expanded in powers of  $\mu$ , then gives  $\lim_{x \rightarrow \infty} c_1 = 0$ , which implies that the coefficient of  $e^x$  in (5.15) approaches zero as  $x \rightarrow \infty$ . Thus,

$$\xi_0 = -\frac{1}{2\Lambda b_\infty} \int_0^\infty \frac{e^{-3y} - e^{-2y}}{y} dy = \frac{1}{2\Lambda b_\infty} \ln \frac{3}{2}.$$

Similarly,  $\lim_{x \rightarrow 0} \{-x^2 dc_1/dx\} = 0$ , which leads to

$$\eta_0 = -\xi_0 - \frac{3(1 + c_\infty)}{4b_\infty}.$$

Finally,

$$c_1 = \frac{1 + c_\infty}{2b_\infty \Lambda x} \left[ 2 - (2 + x) e^{-x} \right] + \frac{1}{2b_\infty \Lambda^2 x} \left[ e^x \int_x^\infty \frac{e^{-2y} - e^{-3y}}{y} dy - e^{-x} \left( \ln \frac{3}{2} + \int_0^x \frac{e^{-y} - 1}{y} dy \right) \right],$$

which is rewritten in terms of standard special functions below (5.18).

**5.2. Summary.** We have derived a two-term asymptotic expansion for the regime in which the buffer does not saturate (EBA), that is,  $\varepsilon_c = O(1)$  and  $\varepsilon_b \gg 1$ . We have expanded  $c$  and  $b$  in terms of  $\mu = \varepsilon_c/\varepsilon_b = \beta/D$  as follows:

$$(5.16) \quad c \sim c_\infty + \frac{1}{\rho} e^{-\rho/\Lambda} + \mu c_1 + O(\mu^2),$$

$$(5.17) \quad b \sim b_\infty + \mu \frac{1}{\rho} (e^{-\rho/\Lambda} - 1) + O(\mu^2).$$

Here  $c_1$  is given by

$$(5.18) \quad c_1 = \frac{1 + c_\infty}{2b_\infty \Lambda x} [2 - (2 + x) e^{-x}] + \frac{1}{2b_\infty \Lambda^2 x} \left[ e^x E_1(2x) - e^x E_1(3x) + e^{-x} \left( E_1(x) + \ln x - \ln \frac{3}{2} + \gamma \right) \right],$$

where  $x = \rho/\Lambda = \rho \sqrt{b_\infty/\varepsilon_c}$ ,  $\gamma \approx 0.5772$  is Euler's constant, and  $E_1(x)$  is the exponential integral,

$$E_1(x) = \int_x^\infty \frac{e^{-y}}{y} dy.$$

**6. The RBA.** In the dimensionless equations, the reaction terms are  $O(1)$ , so the assumption of rapid binding is equivalent to  $\varepsilon_b \ll 1$  and  $\varepsilon_c \ll 1$ . In other words, diffusion of both  $b$  and  $c$  is slow compared to the reaction terms. This is the case, for example, if  $\mu = \beta/D = O(1)$  and  $\varepsilon \ll 1$  due to either a large association rate constant ( $k^+$ ), a large source amplitude ( $\sigma$ ), or both. Note that a sufficiently strong source can compensate for modest binding rates, so the historical name, RBA, is incomplete for the approximation in this regime. The essence of the RBA, as derived in prior work (see section 3.2), is the assumption of local equilibrium. This assumption is certainly true to leading order, as can be seen from formally setting  $\varepsilon_c = \varepsilon_b = 0$  in (4.2) and (4.3) to obtain

$$(6.1) \quad b = \frac{1}{1 + c}.$$

The heuristic derivation of the steady-state RBA can be completed by obtaining a second algebraic relationship between  $b$  and  $c$ . Subtracting (4.3) from (4.2) yields

$$(6.2) \quad \nabla_\rho^2 (\varepsilon_c c - \varepsilon_b b) = 0.$$

Integrating twice with respect to  $\rho$  and using the boundary conditions to determine the integration constants gives

$$(6.3) \quad \varepsilon_c c - \varepsilon_b b = \frac{\varepsilon_c}{\rho} + \varepsilon_c c_\infty - \varepsilon_b b_\infty.$$

Unlike (6.1), relation (6.3) is true whether or not  $\varepsilon_c$  and  $\varepsilon_b$  are small. Indeed, (6.3) is equivalent to the fact that at steady state the flux of total  $\text{Ca}^{2+}$ , bound to buffer and unbound, across any spherical surface centered on the source is equal to the flux entering through the source. Solving (6.1) and (6.3) for  $b$  and  $c$  gives the leading-order approximations (6.6) and (6.7) below, where (6.7) is equivalent to (3.4). Thus, the

steady-state RBA obtained previously in [16] is shown here to be the leading-order solution to the full equations for small  $\varepsilon_b$  and  $\varepsilon_c$ .

In order to obtain higher-order correction terms and to ensure matching of inner and outer solutions, we use (6.3) to eliminate  $c$  in (4.3), giving a differential equation for  $b$  alone:

$$(6.4) \quad \varepsilon_b \nabla_\rho^2 b - \left( \frac{1}{\mu} b^2 + \phi(\rho) b - 1 \right) = 0,$$

where

$$\phi(\rho) = \frac{1}{\rho} + c_\infty - \frac{1}{\mu} b_\infty + 1.$$

If  $\varepsilon_b \ll 1$  and  $\mu = O(1)$ , then (6.4) is a singularly perturbed differential equation. Assuming an outer (large  $\rho$ ) solution of the form

$$(6.5) \quad b^{out} = b_0^{out} + \varepsilon_b b_1^{out} + \varepsilon_b^2 b_2^{out} + \dots,$$

we have the leading-order equation

$$\frac{1}{\mu} (b_0^{out})^2 + \phi(\rho) b_0^{out} - 1 = 0,$$

with positive solution

$$(6.6) \quad b_0^{out} = \frac{\mu}{2} \left[ -\phi(\rho) + \sqrt{\phi(\rho)^2 + 4/\mu} \right].$$

Using relation (6.3) between  $c$  and  $b$ , we have

$$(6.7) \quad c_0^{out} = \frac{1}{2} \left[ -\phi(\rho) + \sqrt{\phi(\rho)^2 + 4/\mu} \right] + \frac{1}{\rho} + c_\infty - \frac{1}{\mu} b_\infty.$$

Note that the outer solution (6.6), (6.7) already satisfies the boundary conditions at  $\rho = 0$  as well as at  $\rho = \infty$  because the conditions at both boundaries were used in obtaining (6.3). In particular, as  $\rho \rightarrow 0$ ,  $b_0^{out} \sim \rho$  and  $c_0^{out} \sim 1/\rho$ , so the boundary conditions at  $\rho = 0$  are satisfied. This is fortunate as there are no free parameters available to use in matching.

Examination of (6.3) reveals that  $b$  neither blows up nor has a boundary layer near  $\rho = 0$ . Thus, the outer solution for  $b$  must be uniformly valid to the origin and match the boundary condition there. One also can calculate the inner solution explicitly, rescaling to introduce a new spatial variable  $x = \rho/\varepsilon_b$ , chosen to balance terms in (6.4), to obtain

$$(6.8) \quad b^{in} \sim (x+2)\varepsilon_b + O(\varepsilon_b^2).$$

This matches the outer solution obtained below to second order.

Using (6.4) and (6.5) we obtain the second-order outer equation,

$$\nabla_\rho^2 b_0^{out} - \left[ \frac{2}{\mu} b_0^{out} b_1^{out} + \phi(\rho) b_1^{out} \right] = 0.$$

Since  $b_0^{out}$  is known, this is an algebraic equation for  $b_1^{out}$ :

$$b_1^{out} = \frac{\nabla_\rho^2 b_0^{out}}{\frac{2b_0^{out}}{\mu} + \phi(\rho)} = \frac{2}{\rho^4 [4/\mu + \phi(\rho)]^2},$$

where for the second equality we have evaluated  $\nabla_\rho^2 b_0^{out}$ .

For small  $\rho$ ,  $b_1^{out} \sim 2$ . Thus, the outer solution satisfies

$$b^{out} \sim \rho + 2\varepsilon_b + O(\varepsilon_b^2)$$

for small  $\rho$ . Rewriting the inner solution (6.8) in terms of the outer variable confirms that the inner and outer solutions match up to  $O(\varepsilon_b)$ .

**6.1. Summary.** We have calculated a two-term asymptotic expansion for the solution to the buffered diffusion equations in the limit of  $\varepsilon_b$  and  $\varepsilon_c$  going to zero, that is, when diffusion of buffer and  $\text{Ca}^{2+}$  are slow compared to reaction. The outer solution expansion (6.5) is valid for all  $\rho$ . This gives for  $b$ ,

$$b \sim \frac{\mu}{2} \left[ -\phi(\rho) + \sqrt{\phi(\rho)^2 + 4/\mu} \right] + \varepsilon_b \frac{2}{\rho^4 [4/\mu + \phi(\rho)]^2} + O(\varepsilon_b^2),$$

and for  $c$ ,

$$c \sim \frac{1}{2} \left[ -\phi(\rho) + \sqrt{\phi(\rho)^2 + 4/\mu} \right] + \frac{1}{\rho} + c_\infty - \frac{1}{\mu} b_\infty + \varepsilon_b \frac{2/\mu}{\rho^4 [4/\mu + \phi(\rho)]^2} + O(\varepsilon_b^2),$$

where

$$\phi(\rho) = \frac{1}{\rho} + c_\infty - \frac{1}{\mu} b_\infty + 1.$$

**7. The nearly immobile buffer approximation (IBA).** In this section, we consider a third case,  $\varepsilon_c = O(1)$  and  $\varepsilon_b \ll 1$ . This occurs if  $\varepsilon$  and  $\beta$  are both  $O(1)$ , while  $D \ll 1$ , that is, if the mobility of  $b$  is small compared to the mobility of  $c$  and to the  $O(1)$  reaction terms.

Although this is a singularly perturbed system, we find again that the outer solution satisfies the inner boundary conditions; the inner solution is omitted for brevity. Beginning again with (4.2) and (4.3), and assuming an (outer) solution of the form

$$\begin{aligned} c &= c_0 + \varepsilon_b c_1 + \varepsilon_b^2 c_2 + \dots, \\ b &= b_0 + \varepsilon_b b_1 + \varepsilon_b^2 b_2 + \dots, \end{aligned}$$

we have the leading-order equations

$$(7.1) \quad \varepsilon_c \nabla_\rho^2 c_0 - (c_0 b_0 + b_0 - 1) = 0,$$

$$(7.2) \quad c_0 b_0 + b_0 - 1 = 0.$$

Obviously,  $\nabla_\rho^2 c_0 = 0$ , so integrating twice and solving for the integration constants using the boundary conditions gives

$$(7.3) \quad c_0 = \frac{1}{\rho} + c_\infty.$$

Thus, to leading order,  $\text{Ca}^{2+}$  behaves as if it were unbuffered. This makes sense, as completely fixed buffer has no effect on the steady-state free  $\text{Ca}^{2+}$  distribution. Furthermore, (7.2) implies that to leading order, the buffer is in equilibrium with the free  $\text{Ca}^{2+}$  and satisfies

$$(7.4) \quad b_0 = \frac{1}{1 + c_0}.$$

**7.1. Second-order results.** The  $O(\varepsilon_b)$ -system for the IBA is given by

$$(7.5) \quad \varepsilon_c \nabla_\rho^2 c_1 - (c_1 b_0 + c_0 b_1 + b_1) = 0,$$

$$(7.6) \quad \nabla_\rho^2 b_0 - (c_1 b_0 + c_0 b_1 + b_1) = 0.$$

Expressing  $b_0$  in terms of  $c_0$  using (7.4) and subtracting (7.6) from (7.5) gives

$$\nabla_\rho^2 \left( \varepsilon_c c_1 - \frac{1}{1 + c_0} \right) = 0.$$

Integrating twice and using the boundary conditions gives

$$c_1 = \frac{1}{\varepsilon_c} \left( \frac{1}{1 + c_0} - \frac{1}{1 + c_\infty} \right) = \frac{1}{\varepsilon_c} (b_0 - b_\infty).$$

Now using expression (7.4) for  $b_0$  in (7.6), we have

$$(7.7) \quad \nabla_\rho^2 \left( \frac{1}{1 + c_0} \right) - \left( \frac{c_1}{1 + c_0} + (c_0 + 1) b_1 \right) = 0.$$

We solve the above equation for  $b_1$  by noting

$$\nabla_\rho^2 \left( \frac{1}{1 + c_0} \right) = \frac{2}{\rho^4 (1 + c_0)^3}$$

and rearranging (7.7) to give

$$b_1 = \frac{2}{\rho^4 (1 + c_0)^4} - \frac{c_1}{(1 + c_0)^2}.$$

Note that  $\lim_{\rho \rightarrow 0} b_1 = 2$ , which means that at second order, the “nearly” immobile buffer is not completely saturated near the source.

**7.2. Summary.** The two-term asymptotic expansion for the case  $\varepsilon_c = O(1)$ ,  $\varepsilon_b \ll 1$ , i.e., when the buffer has low mobility, is given by

$$\begin{aligned} c &\sim c_0 + \varepsilon_b c_1 + O(\varepsilon_b^2), \\ b &\sim \frac{1}{1 + c_0} + \varepsilon_b \left[ \frac{2}{\rho^4 (1 + c_0)^4} - \frac{c_1}{(1 + c_0)^2} \right] + O(\varepsilon_b^2), \end{aligned}$$

where

$$c_0 = \frac{1}{\rho} + c_\infty$$

and

$$c_1 = \frac{1}{\varepsilon_c} \left( \frac{1}{1 + c_0} - b_\infty \right).$$

**8. The linearized equations.** An alternative to the asymptotic methods presented here is the method of linearizing the equations [11, 14, 20] as described in section 3.3. Here we rederive the linear approximation and clarify its relationship to the asymptotic approximations. Substituting  $c = c_\infty + \delta c$  and  $b = b_\infty + \delta b$  into (4.2) and (4.3) gives

$$(8.1) \quad \varepsilon_c \nabla_\rho^2 \delta c - [(1 + c_\infty) \delta b + b_\infty \delta c + \delta c \delta b] = 0,$$

$$(8.2) \quad \varepsilon_b \nabla_\rho^2 \delta b - [(1 + c_\infty) \delta b + b_\infty \delta c + \delta c \delta b] = 0,$$

with boundary conditions

$$\lim_{\rho \rightarrow \infty} \delta c = 0, \quad \lim_{\rho \rightarrow 0} \left( -\rho^2 \frac{d\delta c}{d\rho} \right) = 1, \quad \lim_{\rho \rightarrow \infty} \delta b = 0, \quad \lim_{\rho \rightarrow 0} \left( -\rho^2 \frac{d\delta b}{d\rho} \right) = 0.$$

Dropping the quadratic terms  $\delta c \delta b$  in (8.1) and (8.2) leaves a linear system whose solution leads to the following approximations for  $c$  and  $b$ :

$$(8.3) \quad c = c_\infty + \frac{1}{\rho(1 + \kappa_\infty D)} [1 + \kappa_\infty D e^{-A\rho}],$$

$$(8.4) \quad b = b_\infty + \frac{\beta \kappa_\infty}{\rho(1 + \kappa_\infty D)} [e^{-A\rho} - 1],$$

where

$$(8.5) \quad \kappa_\infty = \frac{1}{\beta(1 + c_\infty)^2}$$

and

$$A^2 = \frac{1 + c_\infty}{\varepsilon_b} (1 + \kappa_\infty D) = \frac{1 + c_\infty}{\varepsilon_b} + \frac{\varepsilon_c}{1 + c_\infty}.$$

When expressed in terms of dimensional quantities, the  $\kappa_\infty$  above is the same as the  $\kappa_\infty$  in (3.7).

Because  $\delta c$  does not remain small but blows up as  $\rho \rightarrow 0$ , dropping the  $\delta c \delta b$  terms in (8.1) and (8.2) requires justification. Subtracting (8.2) from (8.1) gives  $\nabla_\rho^2 [\varepsilon_c \delta c - \varepsilon_b \delta b] = 0$ , and integrating and using the boundary conditions give  $\varepsilon_c \delta c - \varepsilon_b \delta b = \varepsilon_c / \rho$ , that is,

$$(8.6) \quad \delta c = \frac{1}{\rho} + \frac{D}{\beta} \delta b.$$

Substitution into (8.2) gives

$$(8.7) \quad \varepsilon_b \nabla_\rho^2 \delta b - \left[ \left( 1 + c_\infty + \frac{D}{\beta} b_\infty \right) \delta b + \frac{b_\infty}{\rho} + \frac{\delta b}{\rho} + \frac{D}{\beta} \delta b^2 \right] = 0.$$

We now can see that dropping  $\delta c \delta b$  in (8.1), (8.2) corresponds to dropping  $\delta b / \rho$  and  $D\delta b^2 / \beta$  in (8.7). This is justified when  $\delta b \ll b_\infty$ , whether or not  $\delta c$  is small, because then  $D\delta b^2 / \beta \ll Db_\infty \delta b / \beta$  and  $\delta b / \rho \ll b_\infty / \rho$ . This is valid for small  $\rho$  because the latter terms then dominate the other terms in the brackets of (8.7).

There are two limiting cases in which the linear approximation reduces to simpler forms that we have seen already. For large  $\kappa_\infty$ , EBA and the linear approximation

are essentially equivalent. That is, if  $\kappa_\infty \gg 1$ , then, provided  $D = O(1)$ ,  $c_\infty + \delta c$  for the linearized solution (8.3) reduces to the leading-order solution  $c_0$  for the EBA (5.7), and the linear approximation for  $b_\infty + \delta b$  reduces to the second-order solution  $b_0 + \mu b_1$  for the EBA (5.17). This makes sense because large  $\kappa_\infty$  implies  $\beta \ll 1$ , which together with  $D = O(1)$  leads to the EBA. Conversely, when the EBA is valid,  $\delta b \ll b_\infty$  (5.17), and linearization also is valid.

On the other hand, if  $\kappa_\infty$  is not large, then EBA and linearization differ. This will be discussed further in section 9, where the various approximations are compared numerically. Here we just note that in the extreme case of  $\kappa_\infty \rightarrow 0$ , the linear approximation reduces to  $c = c_\infty + 1/\rho$  and  $b = b_\infty$ . Small  $\kappa_\infty$  means that there is very little buffer or it has very low affinity. Therefore,  $\text{Ca}^{2+}$  is effectively unbuffered, and the linear approximation for  $c$  is the same as the leading-order solution  $c_0$  for the IBA (7.3). In this same limit, however, the linear approximation says that buffer is unperturbed, in disagreement with the leading-order IBA solution for  $b$ , which is in equilibrium with  $c$ . Thus, although the condition  $\delta b \ll b_\infty$  does not hold in this region, setting  $\delta b = 0$  leads to the correct equation for  $c$  because the buffer has little effect on  $\text{Ca}^{2+}$ .

Further examination of (8.7) reveals that one can drop only the  $\delta b^2$  term and still have a linear equation for  $\delta b$ :

$$(8.8) \quad \varepsilon_b \nabla_\rho^2 \delta b - \left(1 + c_\infty + \frac{D}{\beta} b_\infty + \frac{1}{\rho}\right) \delta b - \frac{b_\infty}{\rho} = 0.$$

However, the solution is considerably more complex than (8.3) and (8.4) because of variable coefficients, and the approximation is not noticeably improved, so we do not pursue this option further.

**9. Error analysis.** Solving (6.3) for  $c$  in terms of  $b$  and substituting into (4.3) gives the full equations in terms of  $b$  alone,

$$(9.1) \quad \varepsilon_b \nabla_\rho^2 b - \frac{1}{\varepsilon_c} \left[ \varepsilon_b b + \frac{\varepsilon_c}{\rho} + \varepsilon_c c_\infty - \varepsilon_b b_\infty \right] b - b + 1 = 0.$$

Numerical solutions of this equation, denoted by  $b^{full}$ , and associated values of  $c^{full}$  (6.3), are the standard to which we compare the asymptotic approximations developed above (denoted by  $b^{app}$  and  $c^{app}$ ). A finite difference scheme was used to discretize the boundary-value problem defined by (9.1) and (4.7) and the resulting matrix equation was solved using Newton's method.

To compare the approximations,  $b^{app}$  and  $c^{app}$ , to the numerical solutions,  $b^{full}$  and  $c^{full}$ , of the full equations, we calculated an absolute error for  $b$ ,

$$E_{abs} = \left( \sum_i |b_i^{app} - b_i^{full}|^p \right)^{1/p},$$

because  $b$  is bounded, and a relative error for  $c$ ,

$$E_{rel} = \left( \sum_i \left| \frac{c_i^{app} - c_i^{full}}{c_i^{full}} \right|^p \right)^{1/p},$$

because  $c$  is unbounded, where  $p = 1, 2$ , or  $\infty$ . The index  $i$  runs over discretized mesh intervals from the origin to a large value of  $\rho$ . These are very strict error measures,

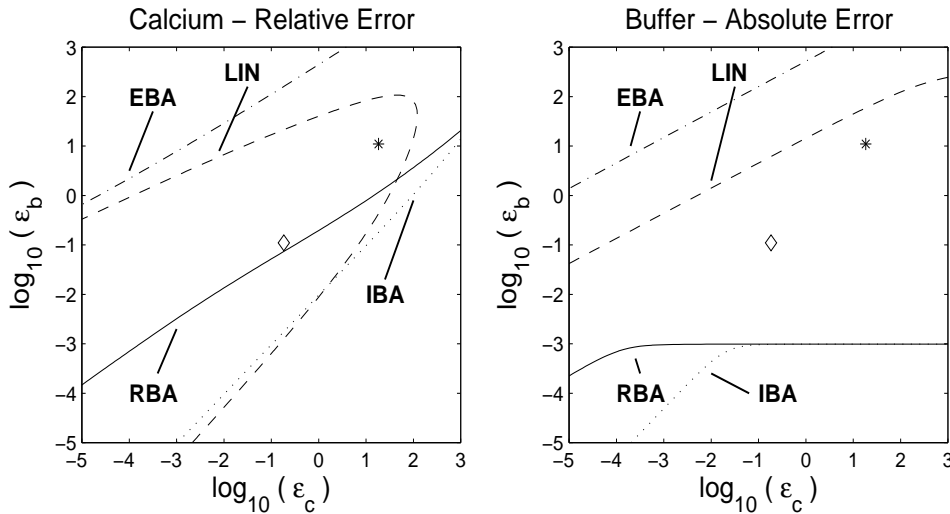


FIG. 9.1. Regions of validity for the three first-order asymptotic approximations and linearization are plotted in the  $(\varepsilon_c, \varepsilon_b)$ -plane. Solid (RBA), dotted (IBA), dot-dashed (EBA), and dashed (LIN) contour lines indicate  $10^{-3}$  relative error and absolute error in  $c$  and  $b$ , respectively. The  $*$  and  $\diamond$  correspond to  $*$  and  $\diamond$  in Figure 4.1. Text is placed on the “good” side of each contour.

since they require the approximate and “exact” solutions to be close both near and far from the source. In Figures 9.1 and 9.2,  $p = 2$ ; little change was detected with  $p = 1$  or  $p = \infty$ .

The asymptotic analysis predicted that EBA would be accurate for  $\varepsilon_b \gg 1$  and  $\varepsilon_c = O(1)$ , or  $\varepsilon_b = O(1)$  and  $\varepsilon_c \ll 1$ . In other words, EBA should be valid when the dimensionless mobility of  $b$  is greater than that of  $c$ , which is confirmed by Figures 9.1 and 9.2. RBA was derived assuming  $\varepsilon_c \ll 1$  and  $\varepsilon_b \ll 1$ , that is, both species have low mobility in comparison to the rate of reaction. RBA is indeed accurate in the lower left corner of the parameter plane, but also for most of the lower right region. However, the right-hand part of the RBA region coincides with that of the IBA, where  $\varepsilon_b$  is small, but  $\varepsilon_c$  is not, as expected from the IBA assumptions. The region of validity of RBA extends into that of IBA because the RBA solution reduces to that for unbuffered diffusion when the buffers are ineffective. Numerically, the IBA region is thus largely redundant to the RBA, but it is useful to distinguish conceptually the subregions of RBA where buffer significantly perturbs the  $c$  profile and where it has little effect. In the latter case, the simpler IBA formulas can be used.

The IBA is not merely of academic interest. Buffers with reduced mobility cause smaller perturbations of the  $\text{Ca}^{2+}$  signal at steady-state (7.3). This is of practical importance experimentally, because  $\text{Ca}^{2+}$  concentration is typically measured using fluorescent dyes, which are exogenous  $\text{Ca}^{2+}$  buffers. For example, conjugating the  $\text{Ca}^{2+}$  indicator dye  $\text{Ca}^{2+}$ green to the large molecule dextran reduces the diffusion coefficient of the dye from  $85 \mu\text{m}^2/\text{s}$  [8] to  $20 \mu\text{m}^2/\text{s}$  [9]. There are trade-offs, however, because stationary dyes tend to distort the transient signal even more than mobile dyes [17].

Overall, for  $\text{Ca}^{2+}$ , EBA and RBA roughly split the  $(\varepsilon_c, \varepsilon_b)$ -plane into two regions:

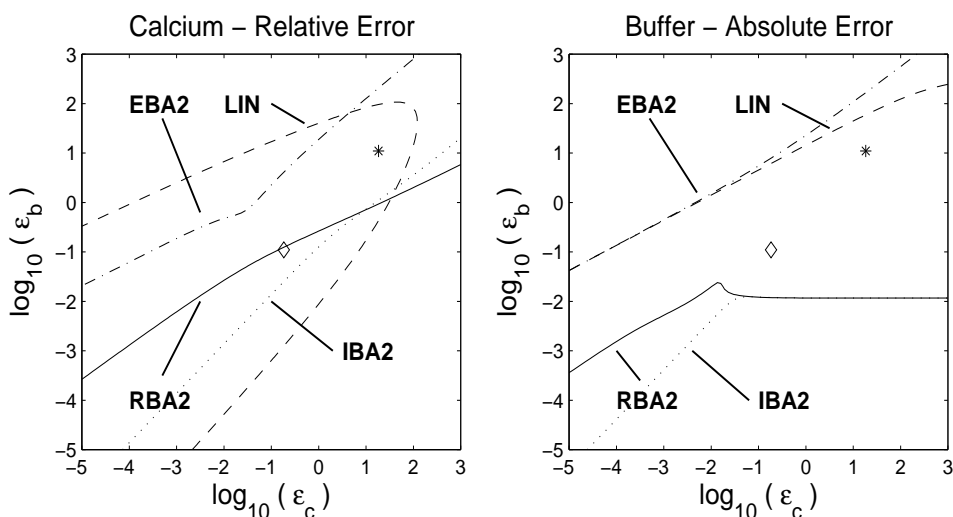


FIG. 9.2. Regions of validity for the three second-order asymptotic approximations are plotted in the  $(\varepsilon_c, \varepsilon_b)$ -plane. Linearization (LIN) replotted from Figure 9.1 for comparison. Solid (RBA2), dotted (IBA2), dot-dashed (EBA2), and dashed (LIN) contour lines indicate  $10^{-3}$  relative error and absolute error in  $c$  and  $b$ , respectively. The  $*$  and  $\diamond$  correspond to  $*$  and  $\diamond$  in Figure 4.1. Text is placed on the “good” side of each contour.

(1) the upper left ( $\varepsilon_c \ll \varepsilon_b$ ), where EBA is valid, and (2) the lower right ( $\varepsilon_b \ll \varepsilon_c$ ), where RBA is valid. This suggests reinterpreting the parameter plane using rotated coordinates,  $\varepsilon$  (cf. (4.8)), which is inversely proportional to  $\sigma^2$  and  $k^+$  and varies along diagonals of slope 1 in the log-log plane, and  $\mu = \varepsilon_b/\varepsilon_c$  (cf. section 5), which varies along diagonals of slope  $-1$ . As  $\mu = D/\beta$  (cf. (4.9), (4.10)), high buffer concentration and mobility are found in the upper left region, where EBA is valid, while low buffer concentration and mobility are found in the lower right region, where RBA and IBA are valid.

Within the upper left region, the EBA contour lines are roughly parallel to the ones shown in Figure 9.1, with slope  $\approx 1$ . Along lines of slope 1,  $D/\beta$  is constant, but when moving toward the lower left, both  $\beta$  and  $D$  decrease. At the same time,  $\sigma$  and/or  $k^+$  increase. Thus, if source strength increases or buffer binding becomes more rapid or buffer mobility decreases, then more buffer is needed to avoid saturation. Similarly, within the RBA region, as buffer concentration increases, the source strength or binding rate must increase to saturate the buffer, even if buffer mobility decreases. Moving horizontally to the IBA region, we see that even a relatively weak source can deplete the buffer if the concentration and mobility are low enough.

The ratio  $\varepsilon_b/\varepsilon_c$  also is proportional to  $\kappa_\infty$  (cf. (8.5)), provided  $D$  and  $c_\infty$  are fixed. The region of accuracy for the linear approximation (LIN) for  $\text{Ca}^{2+}$  intersects both the EBA region, where  $\kappa_\infty$  tends to be large, and the IBA region, where  $\kappa_\infty$  tends to be small. In section 8, we saw that LIN reduces to EBA when  $\kappa_\infty$  is large and, for  $\text{Ca}^{2+}$ , to IBA when  $\kappa_\infty$  is small. In practice, the parameters are more likely to lie in the IBA region because  $D$  is small rather than because  $\beta$  is large, but conceptually,  $\kappa_\infty$  in (8.3) and (8.4) interpolates between two distinct parameter regimes in which (4.2) and (4.3) are nearly linear—one in which buffer is nonsaturating and one in

which buffer is ineffective.

The profiles displayed in Figure 4.1 correspond to points lying between the EBA and IBA/RBA regions (see \* and  $\diamond$  in Figures 9.1, 9.2). When the source is relatively weak, the behavior is more EBA-like, whereas when the source is strong, it is more RBA-like. For the weak source, going to second order significantly improves the accuracy of EBA by allowing partial buffer saturation. For the strong source, going to second order significantly improves the accuracy of RBA by allowing less than complete buffer saturation. IBA profiles (not shown) are similar to those for RBA for both the strong and weak source. Both approximations are better for the strong source than for the weak source, and going to second order does not help either for the weak source. The strong source provides an example where RBA works because  $c$  is nearly unbuffered in spite of the fact that buffer is saturated. The solution is nearly a line of slope  $-1$  in the  $\log(c)$ ,  $\log \rho$  plane, at least up to  $\rho \approx 1$ , i.e.,  $r \approx L$ .

LIN significantly improves on EBA for the weak source; indeed, it is indistinguishable from the exact solution for  $c$  in Figure 4.1. LIN also gives an accurate result for  $c$  when the source is strong, in spite of the fact that  $\delta b$  is not small (cf. section 8) in that case. In fact,  $\delta b$  is so large, that buffer goes negative.

As another illustrative example, extensive use of LIN was made by Pape, Jong, and Chandler [14] in their study of cut skeletal muscle fibers in frogs. These authors added 20 mM EGTA in order to soak up essentially all the  $\text{Ca}^{2+}$  released from internal stores and limit the spread of  $\text{Ca}^{2+}$ . This had two benefits. The  $\text{Ca}^{2+}$  release channels, which are themselves  $\text{Ca}^{2+}$ -sensitive, then were effectively isolated from each other, and the protons that are stoichiometrically liberated from EGTA when it binds  $\text{Ca}^{2+}$  were used to estimate the total  $\text{Ca}^{2+}$  released.

Using their estimated source strength of about 0.15 pA, or even up to an order of magnitude larger, the parameters lie deep in the EBA regime, and LIN, EBA, and EBA2 are indistinguishable both from each other and from the exact solution. In the range 1–10 pA, buffer saturation becomes nonnegligible, but this is captured by EBA2 and LIN. Continuing well beyond the physiological range, 10–100 pA, EBA2 and LIN begin to underestimate the degree of buffer saturation significantly. The results for  $c$  remain qualitatively acceptable even for first-order EBA for all plausible values of source strength. Independent of  $\sigma$ , at these high concentrations of high-affinity buffer, LIN and EBA2 are indistinguishable because  $\kappa_\infty$  is enormous (about 40,000).

Generally, within the EBA region, there is a choice of three approximations. These are leading-order EBA, LIN, and second-order EBA, in order of increasing complexity and increasing accuracy. Whereas at the margins, LIN improves on EBA, by accounting for partial buffer saturation, there is a significant region where the second-order EBA for buffer (5.17) does the same somewhat more simply and as accurately (see Figure 9.2). The second-order EBA for  $\text{Ca}^{2+}$  is too complex to calculate by hand or to afford much insight, but involves readily available standard functions. MATLAB scripts to calculate all the approximations and additional figures are available at <http://mrb.niddk.nih.gov/sherman>.

**10. Discussion.** We have considered the steady-state problem of buffered diffusion of  $\text{Ca}^{2+}$  near a single source and developed asymptotic approximations for three distinct parameter regimes, two studied previously in the biophysical literature (EBA, RBA) and one new (IBA). We have reduced the parameter space from seven dimensional parameters to three dimensionless ones. The three parameter regimes we consider are defined by the dimensionless diffusion coefficients of  $\text{Ca}^{2+}$  and buffer in comparison to each other and to the rate of reaction.

The key dimensionless quantities,  $\varepsilon_c$  and  $\varepsilon_b$ , also capture other parameter relationships observed previously, such as the importance of a strong source for RBA and of high buffer concentration for EBA. The balance of the many physical parameters essentially boils down to whether free buffer can get in to the source fast enough to replace the bound buffer and avoid saturation or whether  $\text{Ca}^{2+}$  overpowers the buffer.

The parametric dependence of the various regimes is clearer perhaps if the alternative dimensionless quantities  $\varepsilon$  and  $\mu = \beta/D$  (cf. section 4) are used. Source strength and binding rate correspond to the  $\varepsilon$  coordinate, whereas buffer concentration and the ratio of the buffer and  $\text{Ca}^{2+}$  diffusion coefficients correspond to the  $\mu$  coordinate.

Furthermore, physical characterizations that were previously assumed in order to derive the RBA (local equilibrium) and the EBA (nonsaturation of buffer) are derived here as consequences of assumptions about the sizes of these parameters. At higher order, the physical assumptions are seen to be only relative, not absolute. Buffer is neither perfectly in equilibrium nor completely saturated at the source in the higher-order RBA, and partial buffer saturation is seen at higher order in the EBA. The systematic mathematical treatment here thus confirms, amplifies, and extends existing biophysical studies.

We also have analyzed the conditions of validity of LIN (solution to the linearized equations), which hold for an impressively large region of the  $(\varepsilon_b, \varepsilon_c)$ -plane, especially for  $c$ , but which are not apparent a priori. We have found that LIN does not require the deviation of  $c$  from its value at  $\infty$  to be small; only the deviation of  $b$  from its value at  $\infty$  need be small. This condition holds in the EBA regime, where the buffer does not saturate. In the IBA regime, where buffer does saturate, but does not have much effect on  $\text{Ca}^{2+}$ , LIN also gives a good approximation for  $c$ , though not for  $b$ .

The results obtained here nearly cover the  $(\varepsilon_b, \varepsilon_c)$ -plane, except near the middle diagonal (Figures 9.1, 9.2). The asymptotic formulas can be extended easily to higher order, but require more complex formulas. The higher-order EBA formulas involve higher-order exponential integrals, while the higher-order RBA formulas involve higher derivatives of the leading-order terms. Note, however, that adding more terms does not necessarily improve the asymptotic approximations if the expansion parameter is not small. Indeed, applying the formulas outside their regions of validity can lead to nonphysical solutions, such as negative buffer concentration in EBA (and LIN) (see Figure 4.1, lower right inset) and nonmonotonic solutions in RBA. Stern [20] has suggested that one can improve LIN numerically by reformulating the equations as integral equations and constructing successive approximations.

Two natural extensions of this work are to multiple buffers and to multiple sources. (For the first-order steady-state RBA with multiple sources, see [3].) Multiple sources are important because  $\text{Ca}^{2+}$  sources often are clustered in cells. For example, the “elementary events” in  $\text{Ca}^{2+}$  release from internal stores, termed “puffs” or “sparks” [1, 5, 18], are probably generated by highly clustered sources. If the density of sources is high enough, the regions of validity will be shifted away from EBA and toward RBA [15]. This is clear when the sources are close enough together to be considered as lumped point sources, but a more detailed analysis of how this transition occurs would be of interest.

The analysis presented here finally needs to be extended to time-dependent cases. Recall that Wagner and Keizer [21] heuristically derived RBA for the time-dependent traveling wave problem. It is interesting to compare the conditions for the validity of the RBA that they derived with those derived here for a point source. Wagner and

Keizer argued that the RBA would be valid when reaction is fast compared to the diffusive time-scale. The reaction time-scale was determined by linearizing the spatially uniform, time-dependent equations, giving  $T_{react} = 1 / (k^+[Ca^{2+}]_{\infty} + k^+[B]_{\infty} + k^-)$ . The diffusion time-scale was determined by  $T_{diff} = L_{wave}^2/D_c$ , where  $L_{wave}$  is the thickness of the wave-front. Replacing  $L_{wave}$  by our length constant  $L$  (section 4), the criterion  $T_{react}/T_{diff} \ll 1$  implies that our  $\varepsilon \ll 1$  provided  $\beta = O(1)$ . If, in addition,  $D = O(1)$ , then RBA indeed will be valid (section 6). Thus, the Wagner–Keizer criterion is a useful necessary condition but is not sufficient; this is fundamentally a two-parameter problem and cannot be reduced to a single ratio. Moreover, while buffer is everywhere in equilibrium with  $Ca^{2+}$ , the dependence on source strength is opposite in the two cases. A traveling wave-front connects two regions in which buffer and calcium are in equilibrium, and, if the transition is gradual enough, they will remain in equilibrium. Thus, the RBA tends to be valid for waves that are broad in traveling-wave coordinates. Note that such waves would be generated by low-amplitude  $Ca^{2+}$  release events. In contrast, the steady-state RBA near a point source tends to be valid when the source amplitude is large. Thus, each new case requires a separate asymptotic treatment. Asymptotic analyses of the time-dependent RBA both near a point source and for traveling waves are forthcoming.

**Acknowledgment.** We thank John Rinzel for insightful discussions of this work and for encouragement to pursue an asymptotic approach.

## REFERENCES

- [1] M. J. BERRIDGE, *Elementary and global aspects of calcium signalling*, J. Physiol. (Lond.), 499 (1997), pp. 291–306.
- [2] M. J. BERRIDGE, *Neuronal calcium signaling*, Neuron, 21 (1998), pp. 13–26.
- [3] R. BERTRAM, G. D. SMITH, AND A. SHERMAN, *A modeling study of the effects of overlapping  $Ca^{2+}$  microdomains on neurotransmitter release*, Biophys. J., 76 (1999), pp. 735–750.
- [4] H. S. CARSLAW AND J. C. JAEGER, *Conduction of Heat in Solids*, 2nd ed., Clarendon Press, Oxford, 1959.
- [5] H. CHENG, W. J. LEDERER, AND M. B. CANNELL, *Calcium sparks: Elementary events underlying excitation-contraction coupling in heart muscle*, Science, 262 (1993), pp. 740–744.
- [6] D. E. CLAPHAM, *Calcium signaling*, Cell, 80 (1995), pp. 259–268.
- [7] J. CRANK, *The Mathematics of Diffusion*, 2nd ed., Clarendon Press, Oxford, 1975.
- [8] M. EBERHARD AND P. ERNE, *Calcium binding to fluorescent calcium indicators: Calcium green, calcium orange and calcium crimson*, Biochem. Biophys. Res. Comm., 180 (1991), pp. 209–215.
- [9] J. P. Y. KAO, *Practical aspects of measuring  $[Ca^{2+}]$  with fluorescent indicators*, Methods Cell Biol., 40 (1994), pp. 155–181.
- [10] J. KLINGAUF AND E. NEHER, *Modeling buffered  $Ca^{2+}$  diffusion near the membrane: Implications for secretion in neuroendocrine cells*, Biophys. J., 72 (1997), pp. 674–690.
- [11] M. NARAGHI AND E. NEHER, *Linearized buffered  $Ca^{2+}$  diffusion in microdomains and its implications for calculation of  $[Ca^{2+}]$  at the mouth of a calcium channel*, J. Neurosci., 17 (1997), pp. 6961–6973.
- [12] E. NEHER, *Concentration profiles of intracellular  $Ca^{2+}$  in the presence of diffusible chelator*, in Calcium Electrogenesis and Neuronal Functioning, Exp. Brain Res. 14, U. Heinemann, M. Klee, E. Neher, and W. Singer, eds., Springer-Verlag, Berlin, 1986, pp. 80–96.
- [13] E. NEHER, *Usefulness and limitations of linear approximations to the understanding of  $Ca^{2+}$  signals*, Cell Calcium, 24 (1998), pp. 345.
- [14] P. C. PAPE, D. S. JONG, AND W. K. CHANDLER, *Calcium release and its voltage dependence in frog cut muscle fibers equilibrated with 20 mM EGTA*, J. Gen. Physiol., 106 (1995), pp. 259–336.
- [15] S. M. ROBERTS, *Localization of calcium signals by a mobile calcium buffer in frog saccular hair cells*, J. Neurosci., 14 (1994), pp. 3246–3262.
- [16] G. D. SMITH, *Analytical steady-state solution to the rapid buffering approximation near an open  $Ca^{2+}$  channel*, Biophys. J., 71 (1996), pp. 3064–3072.

- [17] G. D. SMITH, J. WAGNER, AND J. KEIZER, *Validity of the rapid buffering approximation near a point source for  $\text{Ca}^{2+}$  ions*, Biophys. J., 70 (1996), pp. 2527–2539.
- [18] G. D. SMITH, J. KEIZER, M. STERN, W. J. LEDERER, AND H. CHENG, *A simple numerical model of  $\text{Ca}^{2+}$  spark formation and detection in cardiac myocytes*, Biophys. J., 75 (1998), pp. 15–32.
- [19] J. SNEYD, P. D. DALE, AND A. DUFFY, *Traveling waves in buffered systems: Applications to calcium waves*, SIAM J. Appl. Math., 58 (1998), pp. 1178–1192.
- [20] M. D. STERN, *Buffering of calcium in the vicinity of a channel pore*, Cell Calcium, 13 (1992), pp. 183–192.
- [21] J. WAGNER AND J. KEIZER, *Effects of rapid buffers on  $\text{Ca}^{2+}$  diffusion and  $\text{Ca}^{2+}$  oscillations*, Biophys. J., 67 (1994), pp. 447–456.
- [22] A. ZADOR AND C. KOCH, *Linearized models of calcium dynamics: Formal equivalence to the cable equation*, J. Neurosci., 14 (1994), pp. 4705–4715.